INTERNATIONAL JOURNAL FOR NUMERICAL METHODS IN FLUIDS, VOL. 14, 1111–1130 (1992)

NON-LINEAR INTERACTION OF WATER WAVES WITH SUBMERGED OBSTACLES

RONALD W. YEUNG AND M. VAIDHYANATHAN

Department of Naval Architecture and Offshore Engineering, University of California, Berkeley, CA 94720, U.S.A.

SUMMARY

The interaction of two-dimensional water waves with a fixed submerged cylinder is studied using a finite difference scheme with boundary-fitted co-ordinates. A mixed Eulerian–Lagrangian (MEL) formulation is used to satisfy the fully non-linear free surface conditions. The diffraction of small-amplitude water waves by a cylinder is examined for various wavelengths and amplitudes of the incident wave. Fourier analyses of the incident and diffracted waves are performed to determine their spectra. An example of a large-amplitude wave breaking over a cylinder is also studied. The non-linear numerical solutions are compared with those of experiments and linear theory where appropriate.

KEY WORDS Non-linear waves Diffraction Wave forces Circular cylinder Grid generation Numerical simulation

1. INTRODUCTION

In this paper we study some aspects of the interaction of non-linear water waves with fixed submerged bodies. In the first case we investigate the diffraction of two-dimensional water waves by submerged bodies. Traditionally, calculations have been performed in the frequency domain using linear theory to obtain the so-called reflection and transmission coefficients. Experimental results[1–3] have shown that such theoretical results are not always adequate and fully non-linear simulations would often be necessary. Considerable interest has been shown in the study of non-linear diffraction recently. Second-order results have been obtained by Vada,[4] while fully non-linear simulations have been performed by Cooker *et al.*[5] and Ertekin and Chian[6] for the case of solitary waves and by Cointe[7] for Stokes' second-order waves. Other non-linear solutions have been obtained where the authors were primarily interested in the values of the forces (see e.g. Reference 8). Extreme forces due to breaking waves have been calculated by Brevig *et al.*[9] and Jagannathan[10] for potential flow and by Miyata *et al.*[11] for viscous flow, the last using a marker-and-cell (MAC) method. We conclude by studying as a second example a case of wave breaking in the presence of a cylinder.

We follow the numerical method developed by Yeung and Ananthakrishnan[12] for solving two-dimensional potential free-surface flows. Essentially, the method involves a second-order-accurate finite difference method for solving the Laplace equation in a time-dependent irregular domain using a specially developed boundary-fitted co-ordinate system. A variational method is used for the grid generation, which can handle steep and multivalued free surface profiles. Exact non-linear boundary conditions are used on the free surface, which is advanced in time by using Lagrangian marker particles.[13]

0271–2091/92/091111–20$10.00

Received 2 May 1991
Revised 30 August 1991

The computer code developed for this problem can be actually applied to fixed bodies of arbitrary shape, which could be floating, submerged or bottom-mounted. However, since the incoming waves are generated by a numerical wavemaker at a finite distance from the body, waves reflecting back to the wavemaker would contaminate the solution. A well known linear theory result is that a submerged circular cylinder in deep water has a reflection coefficient of zero, which was originally shown by Dean[14] and later by Ursell[15] and Mehlum.[16] More recently it has been shown by Friis[17] and McIver and McIver[18] that the property is valid up to second order, and a generalization to higher orders has been carried out by Palm.[19] The fact that the reflection coefficient for a circle is almost zero is also well corroborated by the experimental results of Chiu[1] and Grue and Granlund.[2] Numerical results of Vada to second order[4] also indicate the same. Hence we concentrate on this geometry. Cointe *et al.*[20] have considered a way to circumvent the problem of reflected waves by using 'absorbing wavemakers', where the reflected waves are selectively dissipated by a suitable free surface boundary condition, but there appears to be an inconsistency in separating the reflected wave field from the total wave field.

In the present work we present results of numerical calculations where we try to simulate the experiments of Chiu[1] and Grue and Granlund.[2] The experimental observations include the presence of prominent *higher harmonics* downstream of the cylinder. Further, it is observed that the transmission coefficient for the fundamental wave deviates substantially from the theoretical linear result of unity. These deviations are particularly notable when the cylinder submergence is shallow. This is the domain where we conduct our simulations and endeavour to study these phenomena numerically.

It is also of practical interest to calculate the interaction of large-amplitude waves with submerged bodies when the waves evolve into breaking forms. However, there are difficulties involved in setting up the correct initial and boundary conditions for a general time-dependent problem and comparison with experimental data, even if available, would be difficult. We provide here one such example of breaking wave computation, the numerical results of which are compared with those of Brevig *et al.*,[9] who used a boundary integral method. One should also be aware that viscous effects are important in the interaction of large waves with bodies and force calculations from potential flow solutions may be inadequate. The advantage of the finite difference formulation is that the inclusion of viscous effects at a later stage can be relatively easy. The geometry of the domain becomes quite complicated in a breaking wave scenario. The solution of this type of problem will provide a stringent test on the capabilities of the grid generation scheme developed by Yeung and Ananthakrishnan.[21]

2. FORMULATION OF THE PROBLEM

We conduct simulation in a 'wave tank' with the following controllable parameters: the wavemaker frequency ω, the depth of submergence of the centre of the cylinder from the initial undisturbed free surface, h, and the amplitude of a paddle-type wavemaker, A (see Figure 1). The frequency ω determines the wavelength λ (or alternately the wave number k) through the dispersion relation. All variables are non-dimensionalized by the cylinder radius r, the acceleration due to gravity, g, and the density of water, ρ. Using an explicit relationship between the generated wave amplitude a (or a_1) and the paddle amplitude A based on linear theory,[22] we can control the value of the former with desired precision to create small-amplitude waves. Although $r=1$ by our non-dimensionalization, we will retain it in some expressions later, e.g. h/r, to provide a clearer physical meaning of the parameters in question.

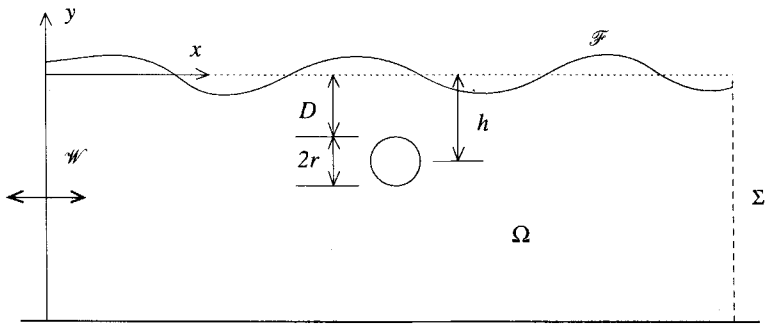

Figure 1. Schematic diagram of the numerical wave tank

With the assumptions of inviscid fluid and irrotational flow we solve the Laplace equation for the velocity potential ϕ,

$$\nabla^2\phi = 0, \tag{1}$$

in the domain Ω shown in Figure 1, with the following boundary conditions.

On the free surface $\mathcal{F}$ the Dirichlet condition for ϕ is obtained by advancing the potential using the dynamic condition

$$D\phi/Dt = \tfrac{1}{2}|\nabla\phi|^2 - y, \tag{2}$$

and its position is updated by the kinematic condition

$$D\mathbf{x}/Dt = \nabla\phi, \tag{3}$$

where D/Dt is the material derivative. These are the well known mixed Eulerian–Lagrangian formulation of Longuet-Higgins and Cokelet.[13]

On the body and bottom of the tank the following no-flux condition is applicable:

$$\phi_n = 0. \tag{4}$$

If a wavemaker is present in the simulation, the following conditions are applied on the left and right boundaries. On the wavemaker surface $\mathcal{W}$, which has a prescribed sinusoidal motion, the appropriate normal velocity is

$$\phi_n = A\omega \sin\left(\frac{2\pi t}{T}\right), \qquad T = \frac{2\pi}{\omega}. \tag{5}$$

On the open boundary the Orlanski condition[23] can be applied, i.e. the potential is advanced in time using the equation

$$\phi_t + c\phi_x = 0, \tag{6}$$

where the phase velocity c is estimated numerically by a scheme to be detailed later. At any particular instant of time the value of ϕ obtained using equation (6) is used as the Dirichlet condition on the open boundary. This condition is only approximate and is expected to be ineffective when short waves ride on long waves. For some discussions we refer to Yeung.[24]

We cannot, however, use a wavemaker to generate the type of waves appropriate for studying the breaking of waves over a cylinder. Large-amplitude motions of the paddle are found to generate propagating transients that would break before reaching the cylinder and thus prevent

long-time numerical simulation. It is possible to superpose wave harmonics in such a way as to generate breaking waves at certain desired positions. Such a procedure leads to a relatively extensive computational domain. Hence, to circumvent the difficulties, we use a domain with spatially periodic boundary conditions. The left and right boundaries are now treated as open boundaries and are allowed to move in time as the motions of the Lagrangian free surface particles on the top of these boundaries dictate. The free surface, bottom, and body boundary conditions remain the same. Hence we have the periodicity condition

$$\phi(x_l, y, t) = \phi(x_r, y, t), \tag{7}$$

where x_l and x_r are the x-positions of the left and right boundaries respectively. The free surface, bottom and body boundary conditions remain the same.

As initial conditions for the wavemaker case we take $\phi = 0$ and $\eta = 0$ on $\mathscr{F}$ and start the wavemaker from rest with zero velocity. For the breaking wave simulation we start with a sinusoidal wave elevation whose wavelength is equal to the length of the domain. The crest of the wave is located at the edges of the domain, while the cylinder is placed below the trough which is at the centre of the domain in the horizontal direction.

Finally, the forces on the cylinder are calculated by direct integration of the pressure based on Euler's integral:

$$p = -\phi_t - \tfrac{1}{2}|\nabla\phi|^2 - y. \tag{8}$$

3. NUMERICAL SCHEME

For the numerical solution of the problem we choose the finite difference method. Even though a boundary integral method would be more efficient for the particular type of problem considered here, we have opted for the finite difference formulation so as to retain the option of including the effects of viscosity. This is in fact being pursued, with initial success reported in Reference 25.

The problem of the varying geometry of the free surface is handled by using boundary-fitted co-ordinates. This method has a higher order of accuracy than 'irregular star' methods, which are the classical alternative.[24] Furthermore, it allows good control of the resolution of the mesh at certain locations in the domain.

3.1. Boundary-fitted co-ordinates

A complete description of the grid generation technique can be found in Reference 21. For continuity of exposition a brief summary will be given here.

To discretize the physical space (x, y) advantageously, we map it into a computational domain (ξ, η) where the grid spacing is uniform and hence the difference formulae have simple forms. The differential operators in the computational space can be determined from the operators in the physical space once the mapping function is known.

There are various ways to do the above mapping. The following method was proposed in Reference 21.

1. An intermediate space called the 'reference space' (α, β) is introduced. This is similar to the physical space but with simplified geometry so that the grids can be generated for this space with ease. The mapping from the computational to the physical space is then the product mapping of the two mappings $(x, y) \rightarrow (\alpha, \beta)$ and $(\alpha, \beta) \rightarrow (\xi, \eta)$. An illustrative example is shown in Figure 2. The notion of reference space was originally introduced by Steinberg and Roache.[26]

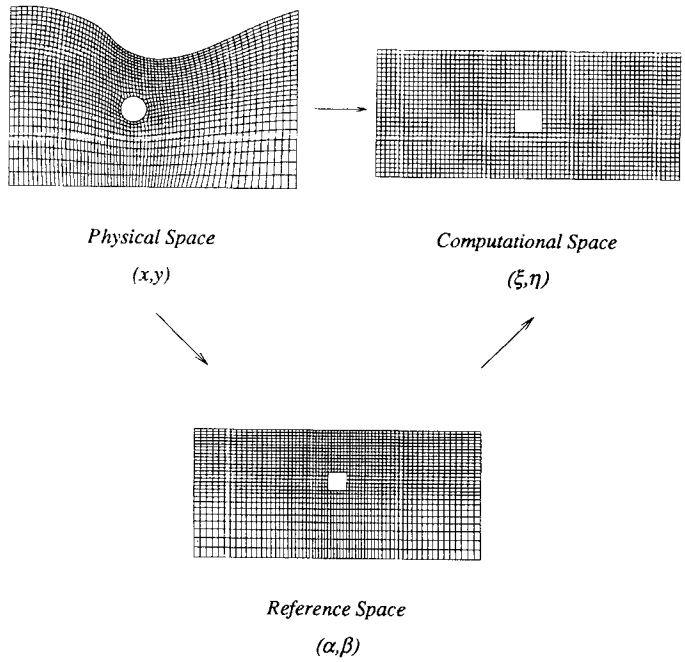

Figure 2. Illustration of the concept of reference space used by Yeung and Ananthakrishnan.[21] The computational space has equidistant nodes. The grid of the physical space resembles the prescribed grid of the reference space. The transformation in two steps as shown proves to be more advantageous

2. The following three integrals are introduced:

$$I_s = \int\int dx\,dy\,|\nabla_{(x,y)}\xi|^2 + |\nabla_{(x,y)}\eta|^2 - \int\int d\alpha\,d\beta\,|\nabla_{(\alpha,\beta)}\xi|^2 + |\nabla_{(\alpha,\beta)}\eta|^2, \tag{9}$$

$$I_v = \int\int dx\,dy(x_\alpha y_\beta - x_\beta y_\alpha), \tag{10}$$

$$I_o = \int\int dx\,dy\,|\nabla_{(x,y)}\xi \cdot \nabla_{(x,y)}\eta|^2 J^3, \tag{11}$$

where $J = x_\xi y_\eta - x_\eta y_\xi$ is the Jacobian of the transformation $(x, y) \rightarrow (\xi, \eta)$. Equation (9) represents a measure of the difference in co-ordinate spacings between the physical and reference spaces. Equations (10) and (11) represent a measure of cell area distribution and orthogonality in the physical space respectively.

3. By equating to zero the first variation of a linear combination of these three integrals, which are functionals of ξ and η, we obtain a set of elliptic partial differential equations for ξ and η.[21] By solving these equations, we obtain the required mapping function. The freedom in choosing the weights on the three functionals gives us great flexibility in generating a grid of certain desired properties. This choice is usually made by utilizing some prior knowledge of the physics of the problem. The grid equations are solved by a mixed over- and underrelaxation procedure.

The above method has proved to be quite powerful in handling domains with rather unwieldy geometries (as Figure 16(d) will show). A high emphasis on I_v and a slight suppression of I_s have

allowed the grids to follow the breaking wave contours while retaining a cell area distribution similar to that of the reference grid. Additionally, this method makes the clustering of grids at appropriate locations more manageable. More examples can be found in Reference 21.

In our implementation the field equation is discretized in the computational space using second-order-accurate difference schemes. The Laplace equation in the computational space (ξ, η) reads as

$$\theta\phi_{\xi\xi} - 2\kappa\phi_{\xi\eta} + \sigma\phi_{\eta\eta} + J^2(P\phi_\xi + Q\phi_\eta) = 0, \tag{12}$$

where $P = \xi_{xx} + \xi_{yy}$, $Q = \eta_{xx} + \eta_{yy}$, $J = x_\xi y_\eta - x_\eta y_\xi$, $\theta = x_\eta^2 + y_\eta^2$, $\kappa = x_\xi x_\eta + y_\xi y_\eta$ and $\sigma = x_\xi^2 + y_\xi^2$. The grid equations, having already been solved, provide the values of the above mapping coefficients. Similar expressions can be arrived at for other derivatives of ϕ.[21] Second-order-accurate one-sided difference operators are used on the boundary, similar to Yeung and Wu.[27] The system of linear equations thus obtained is solved by Gaussian elimination based on LU decomposition.

3.2. Treatment of boundary conditions

The potential on the free surface is obtained by integrating equation (2) using a two-step predictor–corrector method. For the wavemaker case, the free surface wavemaker intersection point is made to satisfy the Neumann condition corresponding to the wavemaker, and its vertical motion is dictated by the free surface kinematic condition. For the small-amplitude motion of the wavemaker we are considering, no singular behaviour is observed at this point. Although the rightmost point on the free surface is a Lagrangian particle, its position is updated at every time step using interpolation to keep its horizontal position constant. This is done to avoid extremely skewed grids at the corner when a wave trough or crest passes through it. Since clustering of free-surface marker particles will lead to instability if the time step is not correspondingly reduced, they are redistributed at every time step. The new positions of the particles are chosen in such a way that the ratio of the arc lengths between nodes to the total arc length of the free surface stays unchanged in time. This is accomplished by interpolation using cubic splines.

To use the approximate open boundary condition equation (6), we follow a scheme similar to that of Jagannathan,[10] which is a modified form of the one proposed by Chan.[28] To obtain the potential at the open boundary at time step $n+1$, we rewrite equation (6) as

$$\phi^{n+1} = \phi^n - cu^n \Delta t, \tag{13}$$

where u is the velocity in the x-direction and the superscripts refer to the time steps. Clearly, we need the phase velocity c. Since this is a time-dependent non-linear process, such a c does not exist in a strict sense, but if the wave field is predominantly of a single frequency, a phase velocity of that wave would be a good approximation. c can be estimated numerically at different free surface points, designated by the index i, neighbouring the free surface and open boundary intersection point by rewriting equation (6) as

$$c_i^n = -\frac{\phi_t}{\phi_x}\bigg|_i^n = \frac{\eta + \frac{1}{2}|\nabla\phi|^2}{u}\bigg|_i^n, \qquad i < i_r, \tag{14}$$

where i_r is the index of the rightmost free surface node. The points where u is very small are discarded and the average of the cs obtained for the remaining points is chosen. Some numerical experimentation showed that the number of points to be averaged over is not very critical.

As a comparative alternative we also used a damping layer similar to that proposed by Baker *et al.*[29] In this method the waves in the far field are damped out artificially. The free surface

boundary conditions (equations (2) and (3)) are rewritten in a more general form as

$$D\phi/Dt = \tfrac{1}{2}|\nabla\phi|^2 - y - \nu(x)\phi, \tag{15}$$

$$D\mathbf{x}/Dt = \nabla\phi - \nu(x)(\mathbf{x} - \mathbf{x}_0), \tag{16}$$

where $\nu(x)$ is an artificial damping parameter and $\mathbf{x}_0$ denotes the initial position of the Lagrangian marker particles, i.e. their position when the fluid is at rest. A specific length on the right side of the fluid domain is demarcated as a damping layer where the above boundary conditions are applied with a positive ν. To the left of the damping layer $\nu(x) = 0$. For monochromatic waves Cointe *et al.*[20] proposes a damping coefficient of the form

$$\nu(x) = \alpha\omega\left(\frac{k}{2\pi}(x - x_d)\right)^2, \tag{17}$$

where α is a dimensionless parameter and x_d is the location of the point where the damping layer begins. Other forms of $\nu(x)$ are also possible.

4. A TEST PROBLEM

Before we proceed to the wave diffraction problems, we must verify whether or not the numerical wavemaker is generating waves that are adequately accurate for our purpose. Hence we carried out some simulations where we solved the wavemaker problem in the absence of obstacles in the tank.

To obtain an incident wave of a desired amplitude, we used linear theory results relating the wavemaker amplitude to the wave amplitude. In the numerical simulations, having specified the estimated paddle amplitude, we used the following procedure to measure the amplitude of the generated wave.

1. The time record of the wave was obtained at many closely spaced stations along the length of the entire tank. Assuming harmonic data, a Fourier series analysis of the wave elevation $\eta(x, t)$ of the form

$$\eta(x, t) = \sum_n a_n(x) \sin(n\omega t + \delta_n) \tag{18}$$

was conducted to obtain $a_n(x)$ at the different stations. The incident wave amplitude a_I referred to previously is a_1 in the above expansion, assuming that there is no reflection from the open boundary. In the presence of a reflected wave of amplitude a_R, with frequency equal to that of the incident wave, a_1 takes the form

$$a_1(x) = \sqrt{[a_I^2 + a_R^2 - 2a_I a_R \cos(2kx + \delta_R)]}, \tag{19}$$

where δ_R is a phase angle. Owing to the limitations of the grid spacing, results obtained for harmonics higher than two are considered unreliable.

2. The evolution of the discrete spectra in time was studied to check for a steady state, i.e. the amplitudes of the first and second harmonics obtained by Fourier analysis for different intervals of time were plotted along the length of the tank. A steady state was assumed to have been reached when the amplitudes, as a function of x, did not change with time.

In Figure 3 we show an example of such a spectrum. The parameters for this case are $\lambda = 7{\cdot}46$ and paddle amplitude $A = 0{\cdot}035$. The incident wave amplitude, according to linear theory, is 0·07. The curves shown are the amplitudes of the first and second harmonics of the wave (a_1 and a_2) as

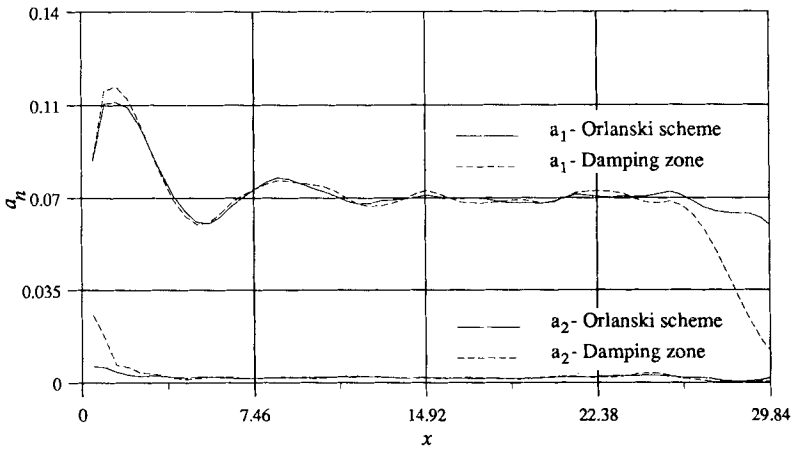

Figure 3. Amplitudes of the first- (a_1) and second- (a_2) harmonic components of the wave record along the length of the tank as obtained by a Fourier series analysis of the wave record between $t=9T$ and $12T$; $\lambda=7{\cdot}46$. The damping zone extends from $x=24{\cdot}54$ to $32{\cdot}00$

a function of the position of the tank. The Fourier series was calculated over the time record from $9T$ to $12T$. The solid curves are obtained using the Orlanski condition described in the previous section, while the dashed curves are obtained using a damping layer. The length of the damping layer was chosen as one wavelength and the value of α in equation (17) was taken as unity.

We make the following observations.

1. The curves did not differ by much when the Fourier series was taken over different time intervals. Hence we can assume that a 'steady state' has been attained over a certain length of the tank.
2. The absence of modulations of the form (19) indicates that reflection from the open boundary, if present, is minimal.
3. The incident wave amplitude is close to the linear theory value for the small values of paddle amplitude which we are considering.
4. The amplitude of the second harmonic is resolved very well in spite of its small value. From Stokes' second-order wave theory[22] the amplitude of the second-order waves should be $a^2k/2=0{\cdot}00206$. The numerically obtained value is very close to this number, though there are slight variations along the length of the tank.
5. Close to the wavemaker we have non-linear evanescent modes, i.e. standing waves, in addition to purely progressive waves. The figure indicates that we should place the body at least two wavelengths away from the wavemaker to avoid such evanescent effects, but to keep the computational efforts low, we did not always follow this criterion.
6. The results obtained using the Orlanski condition and the damping layer are close, except in the damping zone itself where the decay of the amplitude spectrum is clearly noticeable. We preferred to use the former since it requires a smaller computational domain and does not require 'tuning' (i.e. experimentation to find the correct value of damping).

To check the effectiveness of the Orlanski condition, we also plot the variation of the computed phase velocity with time in Figure 4. The approximation is considered good for a reasonable amount of time, but the errors in the computed phase velocity tend to increase after sufficiently long time, especially after the incidence of waves of higher frequencies, as pointed out earlier in

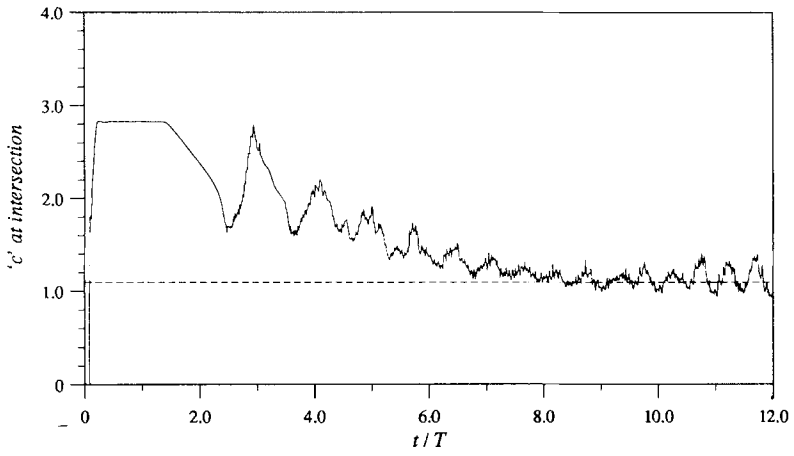

Figure 4. Estimated 'phase velocity' for the open boundary for 12 oscillations of the wavemaker (solid curve). The case shown here corresponds to a wavelength of 7·46 and water depth of 8·0 in the presence of the cylinder. The open boundary is 4·29 wavelengths away from the wavemaker. The dashed line corresponds to the phase velocity of a linear wave of the chosen wavelength

Section 2. The large oscillations at later times are associated with large fluctuations in the velocities at the free surface and open boundary intersection point. The calculated phase velocity is restricted to a maximum value of $\sqrt{d}$, where d is the depth of the tank, since higher values are not valid from physical considerations.[22] Although not shown here, the computed phase velocities in linear calculations are identical to non-linear values, at least up to $t/T=10$.

The numerical calculations did not show sensitivity to the size of the time step as long as the Courant condition $\Delta t \leqslant \Delta x/c$ was satisfied, c being the phase velocity of the primary (fastest) wave. The grid size chosen was found to be adequate to resolve second-order waves through numerical experimentation. As an indication of the accuracy of this type of computation, one can check to see if the energy theorem according to Yeung[24] is satisfied. To do so, we define the following quantities: the energy in the fluid domain as the sum of its kinetic and potential parts,

$$E(t)=\int_{\partial\Omega}\tfrac{1}{2}\phi\phi_n \,\mathrm{d}(\partial\Omega)+\int_{\mathscr{F}}\tfrac{1}{2}\eta^2\,\mathrm{d}x; \tag{20}$$

the work done by the paddle-type wavemaker,

$$W(t)=\int_0^t \mathrm{d}\tau\int_{\mathscr{W}} p\phi_n \,\mathrm{d}y; \tag{21}$$

the energy flux out of the open boundary,

$$W'(t)=\int_0^t \mathrm{d}\tau\int_{\Sigma} p\phi_n \,\mathrm{d}y; \tag{22}$$

and finally the relative error

$$\mathscr{E}(t)=\frac{W(t)+W'(t)-E(t)}{W(t)+W'(t)}, \tag{23}$$

which should be close to zero for an accurate numerical computation. In the above equations Ω is the fluid domain, $\partial\Omega$ is its boundary and Σ is the open boundary (see Figure 1). In Figure 5 the

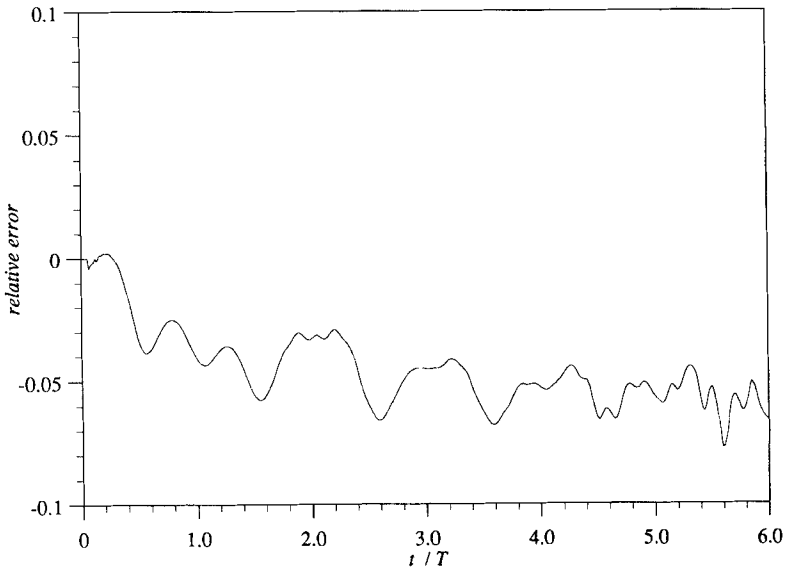

Figure 5. Relative error $\mathscr{E}$ (equation (23)) plotted as a function of time; $\lambda = 16$, paddle amplitude equals 0·05

function $\mathscr{E}(t)$ is shown. The parameters for the problem are $\lambda = 16$, length of the tank, 32, and $A = 0{\cdot}05$. The size of the grid is 80×20. We see that the errors are within 5% until the open boundary condition begins to fail around $t/T = 7$.

In all the cases with the cylinder we used a 119×27 grid. Unlike the case with just the wavemaker alone, where the grid was uniform in both directions, we used closely spaced grids near the cylinder and coarser grids downstream. This gave higher energy losses owing to numerical dissipation caused by the coarse grids.

5. RESULTS AND DISCUSSION

We will divide this study into three parts, the first two corresponding to experimental works which the computations attempt to reproduce, and the breaking wave simulation will be discussed in the third.

The objectives of the two experimental works were slightly different. Chiu[1] conducted extensive experiments for various values of submergence of the cylinder and wavelengths and tested the region of validity of linear theory. He found marked deviations for shallow submergence where second and higher harmonics of the incident wave were generated downstream of the cylinder. Although he realized the importance of the wave slope, all his experiments were conducted with small-amplitude waves since his objective was to compare with the linear theory results of Ogilvie.[30] In addition to determining the region of validity of linear theory, Grue and Granlund[2] also determined the region where second-order solutions[4] were adequate and proceeded to analyse the strong, local, non-linear behaviour in the presence of large-amplitude waves.

In the following two subsections we will describe the results of the numerical simulations, attempting to capture the non-linear phenomena observed in the experiments. In Section 5.3 we will discuss a case similar to one studied by Brevig *et al.*[9] and compare our results with their boundary-integral method solutions. For all the simulations described here, the length of the tank, the depth of the tank and the distance between the wavemaker and the centre of the cylinder

(see Figure 1) were held fixed at 32, 8 and 16 respectively. This configuration is deemed sufficient to represent the case of deep water for the wavelengths that we choose to study.

5.1. *Effect of wavelength and submergence*

The cases studied in this subsection will correspond to the experiments of Chiu.[1] One of the primary conclusions of both experiments was that the non-linearities are important only when the gap above the cylinder is less than one radius (i.e. $h/r < 2{\cdot}0$). A few numerical experiments showed that this was indeed true. Hence we chose the cases corresponding to the shallow submergence values of $h/r = 1{\cdot}5$ and $1{\cdot}275$ as used by Chiu.[1] For each of these submergence values four different wavelengths were tested. Since we are using a finite difference method, high resolution of the grids near the cylinder forces us to have closely distributed nodes on the free surface, which in turn necessitates smaller time steps to satisfy the Courant condition $\Delta t \leqslant \Delta x/c$, c being the phase velocity of the fundamental wave. Hence we confine ourselves to $\lambda \leqslant 16$ for our study to keep the computational time within reasonable limits. A summary of the different cases studied is presented in Table I.

The simulation can normally continue until errors due to the approximate open boundary (equation (6)) cause incorrect wave elevations. This begins to happen when higher-order waves arrive at the open boundary. As shown in Table I, simulations could not be continued for a long time for the $h/r = 1{\cdot}275$ cases and hence the diffracted waves downstream could not be analysed. However, the simulation was long enough to determine the 'steady state' oscillatory forces for cases S-1, S-3 and S-5 of Table I.

An illustration of the wave pattern is quite instructive at this time. In Figures 6–8 we show how the wave pattern changes with the submergence of the cylinder. In non-dimensional units the cylinder is at $x = 16$, the origin corresponding to the mean wavemaker position, and the wavelength is 7·46 for all three cases. The figures show the instantaneous free surface elevations at every 4/75th of a period starting from $t = 4T$ (see equation (5)) and ending at $t = 8T$, t being the non-dimensional time. In Figure 6 the cylinder is deeply submerged ($h/r = 2{\cdot}0$). No non-linear effect is apparent in the figure or in the analysis of the data. For a slightly more shallow submergence ($h/r = 1{\cdot}5$, Figure 7) the presence of the second harmonic riding over the primary wave is clearly visible. In such a situation second-order theory in small-wave-amplitude expansion[4] would be expected to give good results. The necessity of fully non-linear simulations become apparent with an inspection of Figure 8. Here numerous short waves are generated every time the

Table I. Description of the cases studied. These correspond to the shallow submergence cases studied by Chiu[1]

Case	h/r	Paddle amplitude	kr	$2kh$	λ	Length of simulation
S-2	1·500	0·035	0·8417	2·5251	7·46	12 periods
S-4		0·035	0·6066	1·8198	10·35	8 periods
S-6		0·050	0·4981	1·4943	12·61	8 periods
S-8		0·050	0·3976	1·1928	15·80	6 periods
S-1	1·275	0·035	0·8417	2·1479	7·46	Short waves develop after 9 periods
S-3		0·050	0·6024	1·5481	10·35	Short waves develop after 6 periods
S-5		0·050	0·4971	1·2707	12·61	Wave breaks after 4·5 periods
S-7		0·050	0·3915	0·9983	16·05	Wave breaks after 1·5 periods

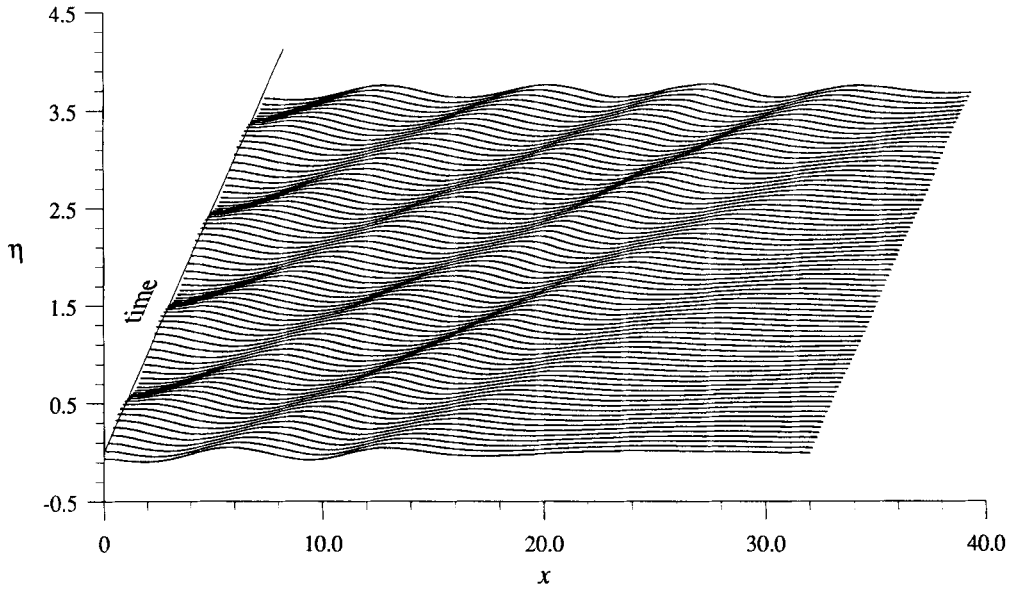

Figure 6. Wave elevations during $4T$–$8T$ in 75 steps; $\lambda/r = 7{\cdot}46$, $h/r = 2{\cdot}0$

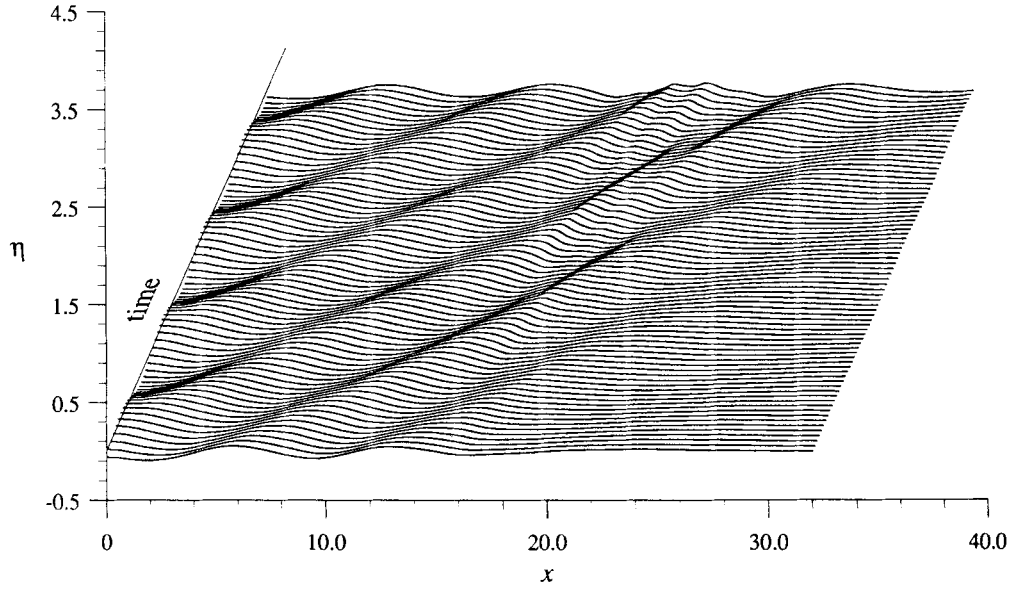

Figure 7. Wave elevations during $4T$–$8T$ in 75 steps; $\lambda/r = 7{\cdot}46$, $h/r = 1{\cdot}5$

wave crest passes over the cylinder. Eventually, waves too small to be resolved by the grid are generated and the simulation has to be stopped.

In his experiments Chiu[1] had wave probes located upstream and far downstream of the cylinder. A Fourier analysis of the time record was conducted to obtain the wave spectrum. Since computed records are always limited in time, we use the analysis procedure described in the

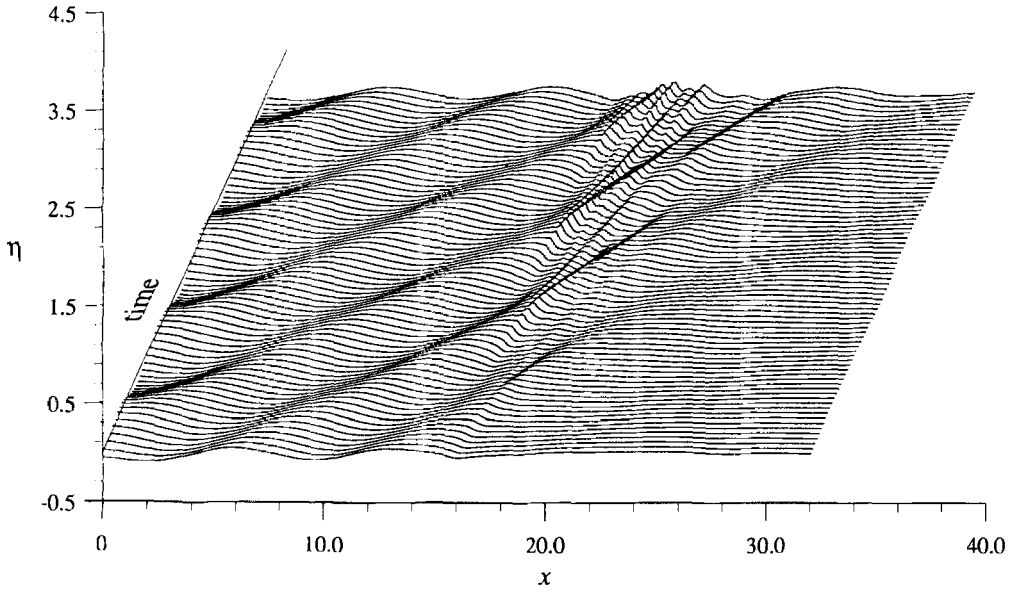

Figure 8. Wave elevations during $4T$–$8T$ in 75 steps; $\lambda/r = 7{\cdot}46$, $h/r = 1{\cdot}275$

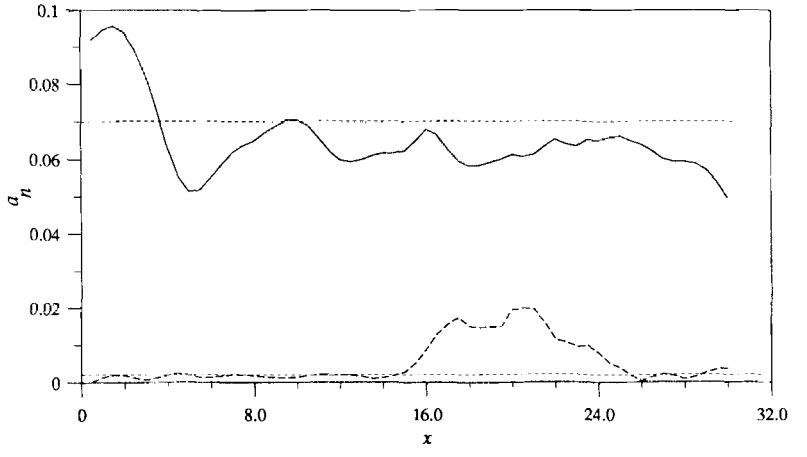

Figure 9. Amplitudes of the first and second harmonics of the transmitted wave (solid and dashed curves respectively) as obtained by Fourier series analysis of the wave elevation, plotted along the length of the tank (case S-2). The horizontal dotted lines show the amplitude of the first-order wave from the linear wavemaker solution and the corresponding Stokes second-order component

previous section (equation (18)). For values of x upstream of the cylinder we denote the value of $a_n(x)$ by a_{1n} and for points downstream of the cylinder by a_{1n}, and $a_1 \equiv a_{11}$. In Figure 9 an example of such a spectrum is shown. The curves shown are the amplitudes of the first- and second-harmonic waves (a_1 and a_2) as a function of the position in the tank, obtained by Fourier series analysis of the time record between $t = 5T$ and $7T$. A variation in the primary wave amplitude upstream of the cylinder (a_{11}) is due to a standing wave generated close to the wavemaker. It

should also be noted that there is no second-order wave component upstream of the cylinder, except for the Stokes' component ($a_{12} = \frac{1}{2}a_1^2 k$), implying that the higher harmonics are generated only downstream of the cylinder.

As previously mentioned, for the shallow submergence case simulations could not be carried out long enough for steady state results to be reached. For $h/r = 1{\cdot}5$ the results of the above analysis are presented in Figure 10. The values plotted are a_{Tn}^2/a_I^2, where a_{Tn} is the amplitude of the first and second-harmonic components in the diffracted wave as obtained by Fourier analysis. Good agreement with the experimental results can be seen. It should also be noted that the transmission coefficient for the first harmonic is much less than unity, the value predicted by linear theory.

A Fourier analysis of the computed force was conducted to obtain the amplitudes of different harmonics. The first-order vertical and horizontal components are almost the same. For $h/r = 1{\cdot}5$ the second-order components are very small. Difficulty was experienced in obtaining second-order forces for $h/r = 1{\cdot}275$ owing to the short duration of the simulation. Larger-amplitude waves and much finer grids would be necessary to obtain reliable results for the higher-order components of the force. The vertical force function is shown in Figure 11. Here we have adopted the non-dimensionalization used by Chiu,[1] whose non-dimensional force function $\mathscr{F}$ is related to ours (denoted by F) by $\mathscr{F} = F/\lambda a_1$. Note that such a non-dimensionalization of force assumes linearity. Experiments show good agreement of forces with linear theory results for $h/r = 1{\cdot}5$, as do our computations. Marked differences in the vertical and horizontal forces were observed in the experiments only for case S-7 ($h/r = 1{\cdot}275$, $\lambda/r = 16{\cdot}05$). However, owing to the occurrence of wave breaking at about $t = 1{\cdot}5\,T$, we were unable to achieve *steady state* results for this case.

It is interesting to observe the mechanism of the wave breaking when a long wave passes over a shallowly submerged cylinder. For case S-7 the velocity vectors and the surface elevation a few time steps before breaking are shown in Figure 12. One can observe the interaction of the

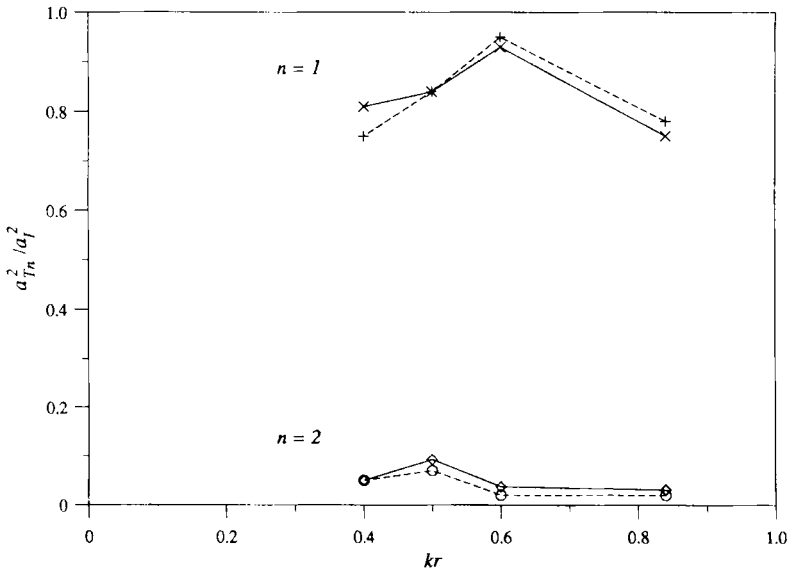

Figure 10. Squares of the first-order (upper curves) and second-order (lower curves) components in the transmitted wave, non-dimensionalized by the incident wave amplitude a_1. The solid curves correspond to the computed values and the dashed curves correspond to the experimental results of Chiu[1]

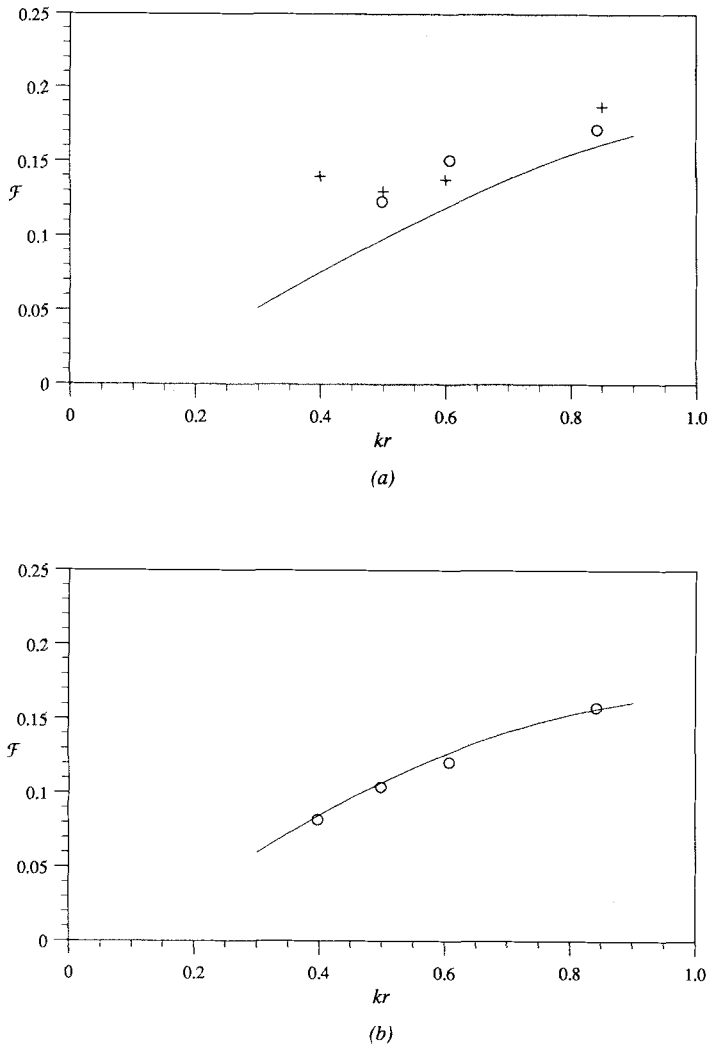

Figure 11. Force coefficients for (a) $h/r = 1{\cdot}275$ and (b) $h/r = 1{\cdot}5$ as a function of kr: ——, linear theory;[30] +, experiment;[1] ○, computed values

accelerated backflow of the outgoing wave in the shallow water region above the cylinder meeting the steepening incoming crest to form a small 'shock' wave just upstream of the point of minimum submergence. For deeper submergences of the cylinder, this splash-like phenomenon generates small ripples downstream of the cylinder as the crest passes over it (Figures 7 and 8).

5.2. *Effect of wave slope*

Grue and Granlund[2] studied the diffraction of an incident Stokes wave by a submerged cylinder. To analyse the result, they made the following decomposition of the wave field.

The incoming wave is a small-amplitude Stokes wave whose surface elevation is given by

$$\eta(x, t) = a\cos(kx - \omega t) + \tfrac{1}{2}a^2 k\cos[2(kx - \omega t)], \tag{24}$$

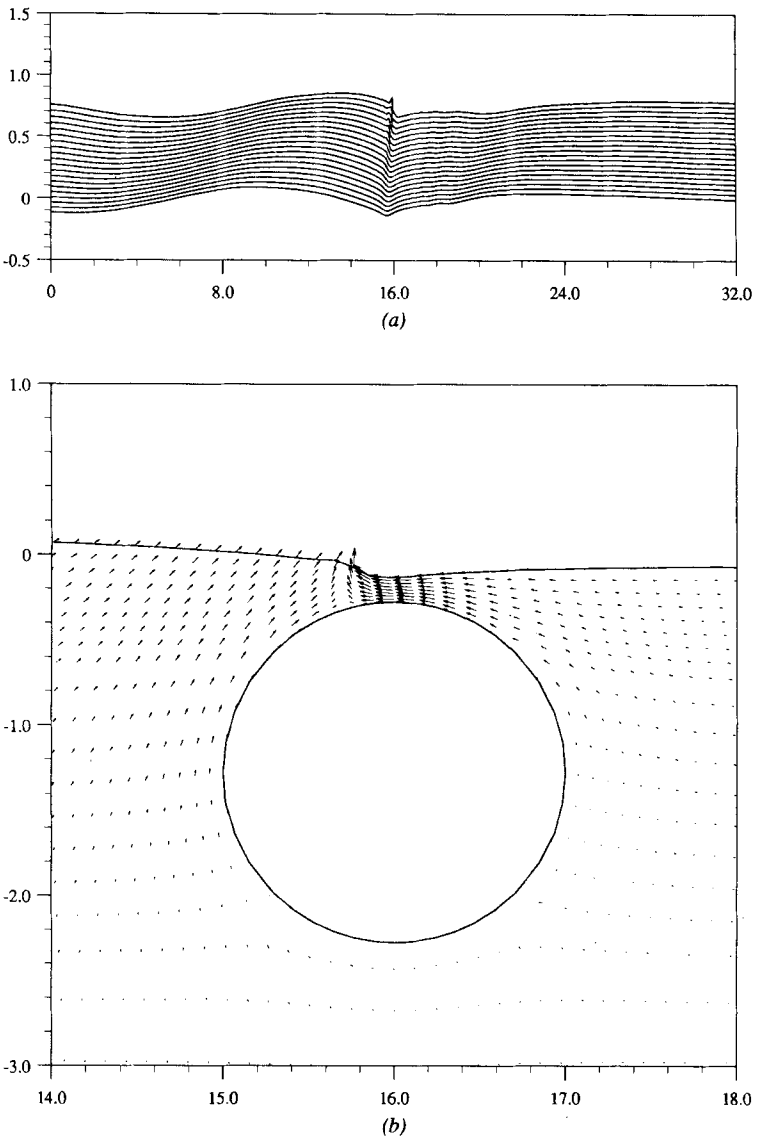

Figure 12. Long wave breaking over a shallowly submerged cylinder ($h/r = 1{\cdot}275$, $\lambda/r = 16{\cdot}05$): (a) wave elevations at time steps 213–232, $\Delta t = T/150$; (b) velocity vectors at $t/T = 1{\cdot}5$

and downstream from the cylinder, besides a Stokes wave of reduced amplitude, there is a free wave of twice the frequency as well as higher-order modes. The surface elevation is therefore given by

$$\eta(x, t) = a_1 \cos(kx - \omega t + \delta_1) + \tfrac{1}{2} a_1^2 \cos[2(kx - \omega t + \delta_1)] + a_2 \cos(4kx - 2\omega t + \delta_2) + \text{higher-order modes}, \tag{25}$$

where a_2 is the amplitude of the free wave.

The experimental results show that for $0{\cdot}2 < a/D < 0{\cdot}6$ and $0{\cdot}3 < kr < 1{\cdot}3$, a_2/r is a function of kr and D/r only, where $D = h - r$ is the clearance between the cylinder and the undisturbed free surface. Thus contrary to the second-order results of Vada,[4] which predicted a quadratic relationship, a_2 does not change with the variation of a for $a/D > 0{\cdot}2$.

We conducted similar numerical experiments for $h/r = 1{\cdot}5$ and $ak = 0{\cdot}3976$ and measured a_2 by using the Fourier method described in Section 3.1 to obtain the coefficients as defined by equation (25). We were successful in capturing the 'saturation' phenomenon, which can be seen in Figure 13. Grue and Granlund[2] observed wave breaking over the cylinder at $ak = 0{\cdot}085$. In our simulations breaking occurs for $0{\cdot}075 < ak < 0{\cdot}085$. It should be mentioned here that the boundary integral method of Cointe *et al.*[7] has also reproduced these non-linear phenomena.

5.3. Wave breaking over a cylinder

In the above cases we observed that the breaking of waves is one of the limiting factors in the numerical study of the non-linear phenomena. Wave breaking is an important non-linear

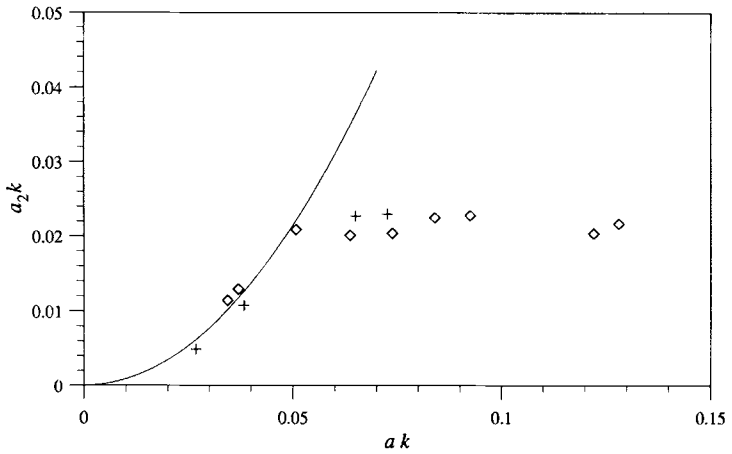

Figure 13. Growth in amplitude of the second-order free wave with increase in amplitude of the incident wave: ——, second-order theory;[4] ◇, experiment;[2] +, present method

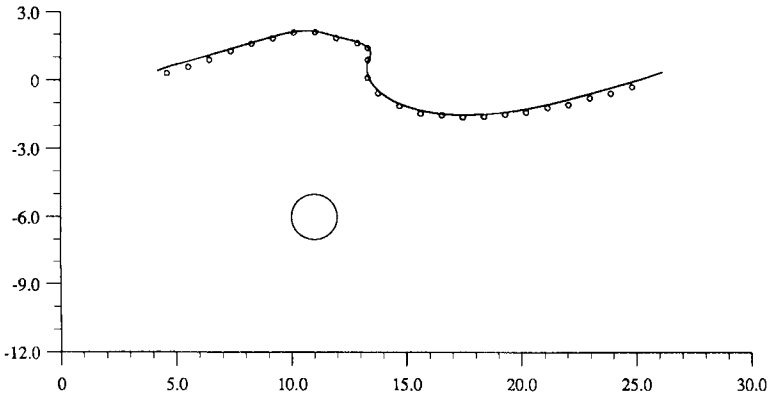

Figure 14. Comparison of wave elevations computed by our method and boundary integral method. The solid curve is the elevation after $0{\cdot}356T$, while the dots represent $t = 0{\cdot}357T$, T being the period of the wave

phenomenon in its own right and deserves special study.[25] Ideally, one would like to observe the breaking of an incoming stream of waves, but the breaking of the early transients makes this approach impractical for numerical study. Hence less realistic, but numerically more appealing, periodic boundary conditions are used to study the breaking of large-amplitude waves.

Brevig *et al.*[9] conducted a comprehensive set of calculations for breaking waves over fixed and freely moving submerged circular cylinders using an integral equation method. More extensive calculations for free-surface-piercing bodies have been conducted by Grosenbaugh and Yeung.[31] We will try to reproduce here one of the cases presented in Reference 9 to demonstrate the ability of our finite difference method to handle such extreme situations also.

In the case presented here we have a cylinder of unit radius in a water depth of 12 under a wave of length 22. The submergence of the cylinder centre is 6 and the amplitude of the wave is 2. At the first time step we impose the velocity potential of a linear progressive wave of a chosen amplitude and wavelength on the *actual free surface* and solve the boundary value problem subject to periodicity conditions in the presence of the cylinder. The solution thus obtained is taken to be the initial condition and the free surface is allowed to evolve from there. We were successful in performing simulations for a short time after the free surface becomes multivalued and our results match with the boundary element results of Brevig *et al.*,[9] who also used the same type of initial condition. The results are presented in Figures 14–16. Unlike the case of the integral equation method, we can now obtain a full description of the details of the flow field as part of the solution processing, thus enabling one to have a better grip of the flow physics. Figure 16 in particular demonstrates well the capability of our grid generation technique in handling the geometry of the type of flow encountered.

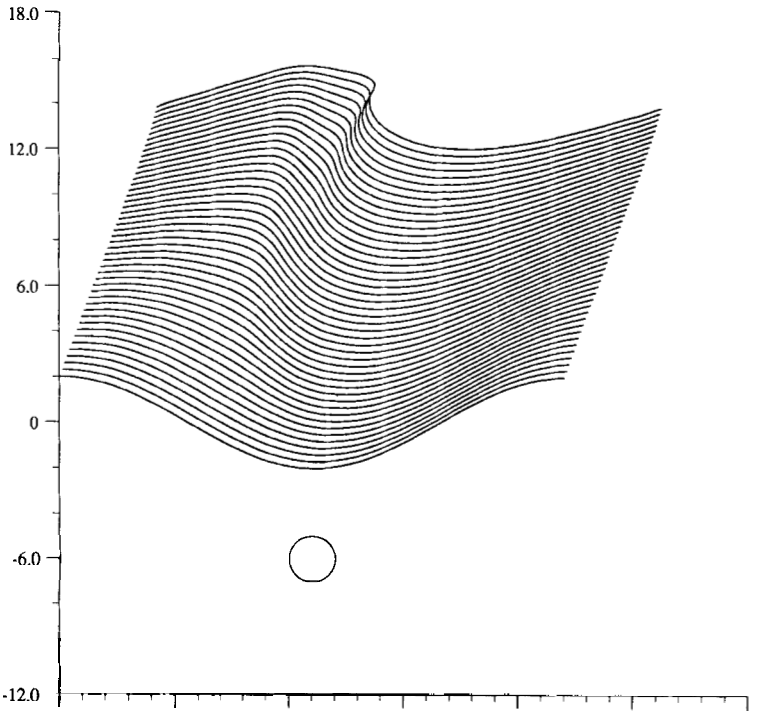

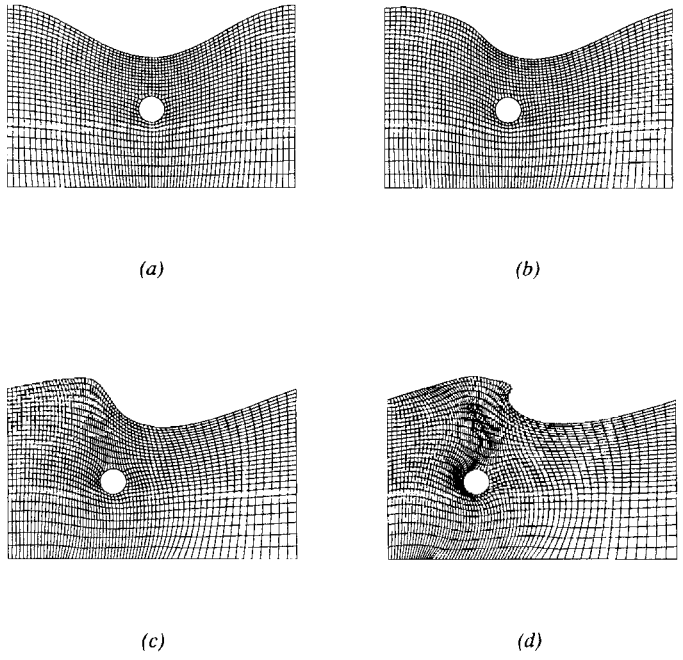

Figure 16. The physical domain at various stages of breaking wave propagation over a cylinder: (a) $t=0$; (b) $t=0{\cdot}12T$; (c) $t=0{\cdot}24T$; (d) $t=0{\cdot}36T$

6. CONCLUSIONS

Two-dimensional problems concerning the non-linear interaction of water waves with submerged obstacles were studied using a finite difference method. The subject of study involves the ability to handle radiation, diffraction, wave breaking and open boundaries.

Our numerical results show good agreement with experimental results and analytical results where applicable. Good predictions of the forces and transmission coefficients have been obtained and in particular the 'saturation' phenomenon of the second-order free wave downstream of the cylinder has been accurately reproduced. Although not as computationally efficient as boundary integral methods, the present method can serve as a foundation for future works to include the effects of viscosity, which could be important in some of the cases studied here. Owing to the versatility of our grid generation technique, fairly complicated geometries have been tackled, including scenarios where the waves are multivalued functions.

Wave breaking and the open boundary condition prove to be limiting factors in long time simulations. For studying the diffraction of waves over bodies other than circular cylinders, there also exists a difficulty in creating an ideal incident wave that would not be contaminated by reflection from the body. Absorbing boundaries can be a promising means of overcoming some, but not all, of these difficulties.

ACKNOWLEDGEMENTS

This research was primarily supported by the Office of Naval Research under contracts N00014-91-J1614 and N00014-91-J1155. Partial support by Research and Development Grants from Cray Computer Inc. and the International Business Machines Corp. is also acknowledged.

REFERENCES

1. H. Chiu, 'Diffraction of water waves by a submerged circular cylinder', *College of Engineering Rep. NA-73-4*, University of California, Berkeley, CA, 1973.
2. J. Grue and K. Granlund, 'Impact of nonlinearity upon waves travelling over a submerged cylinder', *Proc. 3rd Int. Workshop on Water Waves and Floating Bodies*, Woods Hole, MA, 1988, Dept of Ocean Engineering, Mass. Inst. of Technology, pp. 57–60.
3. J. Grue, 'Nonlinear water waves at a submerged obstacle or bottom topography', *Preprint Ser. 2*, Institute of Mathematics, University of Oslo, 1991.
4. T. Vada, 'A numerical solution of the second-order wave diffraction problem for a submerged cylinder of arbitrary shape', *J. Fluid Mech.*, **174,** 23–37 (1987).
5. M. J. Cooker, D. H. Peregrine, C. Vidal and J. W. Dold, 'The interaction between a solitary wave and a submerged semicircular cylinder', *J. Fluid Mech.*, **215,** 1–22 (1990).
6. R. C. Ertekin and C. Chian, 'Numerical solution of some solitary-wave and submerged-obstacle interaction problems', *Proc. 9th Int. Conf. on Offshore Mechanics and Arctic Engineering*, Houston, TX, 1990, ASME, pp. 255–262.
7. R. Cointe, 'Nonlinear simulation of transient free surface flows', *Proc. 5th Int. Conf. on Numerical Ship Hydrodynamics*, Hiroshima, 1989, Hiroshima University, pp. 239–250.
8. P. K. Stansby and A. Slaouti, 'On non-linear wave interaction with cylindrical bodies: a vortex sheet approach', *Appl. Ocean Res.*, **6,** 108–115 (1984).
9. P. Brevig, M. Greenhow and T. Vinje, 'Extreme wave forces on submerged cylinders', *Proc. 2nd Int. Symp. on Wave and Tidal Energy*, Cambridge, 1981, pp. 143–166.
10. S. Jagannathan, 'Nonlinear free surface flows and open boundary conditions', *Ph.D. Thesis*, Department of Naval Architecture and Offshore Engineering, University of California, Berkeley, CA, 1985.
11. H. Miyata, H. Kajitani, M. Zhu and T. Kawano, 'Nonlinear forces caused by breaking waves', *Proc. 16th Symp. on Naval Hydrodynamics*, Berkeley, CA, 1986, National Academy Press, Washington, D.C., pp. 514–536.
12. R. W. Yeung and P. Ananthakrishnan, 'Solution of nonlinear water-wave and wave–body interaction problems using a new boundary-fitted coordinates method', *Proc. 4th Int. Workshop on Water Waves and Floating Bodies*, Øystese, 1989, Dept. of Mathematics, University of Oslo, pp. 269–274.
13. M. S. Longuet-Higgins and E. D. Cokelet, 'The deformation of steep surface waves on water. I. A numerical method of computation', *Proc. R. Soc. Lond. A*, **350,** 1–26 (1976).
14. W. R. Dean, 'On the reflexion of surface waves by a submerged circular cylinder', *Proc. Camb. Phil. Soc.*, **44,** 483–491 (1948).
15. F. Ursell, 'Surface waves on deep water in the presence of a submerged circular cylinder. I', *Proc. Camb. Phil. Soc.*, **46,** 141–152 (1950).
16. E. Mehlum, 'A circular cylinder in water waves', *Appl. Ocean Res.*, **2,** 171–177 (1980).
17. A. Friis, 'Second order diffraction forces on a submerged body by second-order Green function method', *Proc. 5th Int. Workshop on Water Waves and Floating Bodies*, Manchester, 1990, Dept. of Mathematics, University of Manchester, pp. 73–76.
18. M. McIver and P. McIver, 'Second-order wave diffraction by a submerged circular cylinder', *J. Fluid Mech.*, **219,** 519–529 (1990).
19. E. Palm, 'On non-linear reflection from a submerged, circular cylinder', *Proc. 6th Int. Workshop on Water Waves and Floating Bodies*, Woods Hole, MA, 1991, Dept. of Ocean Engineering, Mass. Inst. of Technology, pp. 205–206.
20. R. Cointe, P. Geyer, B. King, B. Molin and M. Tramoni, 'Nonlinear and linear motions of a rectangular barge in a perfect fluid', *Proc. 18th ONR Symp. on Naval Hydrodynamics*, Ann Arbor, MI, 1990, National Academy Press, Washington, D.C., pp. 85–99.
21. R. W. Yeung and P. Ananthakrishnan, 'Numerical grid generation for water-wave problems using reference space', *Rep. NA92-2*, Dept. of Naval Architecture and Offshore Engineering, University of California, Berkeley, 1992.
22. J. V. Wehausen and E. V. Laitone, 'Surface waves', in *Handbuch der Physik, Vol. 9*, Springer-Verlag, Berlin, 1960, pp. 446–814.
23. I. Orlanski, 'A simple boundary condition for unbounded hyperbolic flows', *J. Comput. Phys.*, **21,** 251–269 (1976).
24. R. W. Yeung, 'Numerical methods in free-surface flows', *Ann. Rev. Fluid Mech.*, **14,** 395–442 (1982).
25. R. W. Yeung, 'Nonlinear bow and stern waves—inviscid and viscous solutions', in *Mathematical Approaches in Hydrodynamics*, SIAM, Philadelphia, PA, 1991, pp. 349–369.
26. S. Steinberg and P. J. Roache, 'Variational grid generation', *Numer. Methods Partial Differ. Eqns.*, **2,** 71–96 (1986).
27. R. W. Yeung and C.-F. Wu, 'Nonlinear wave-body motion in a closed domain', *Computers and Fluids*, **7,** 351–370 (1989).
28. R. K.-C. Chan, 'Finite difference simulation of the planar motion of a ship', *Proc. 2nd Int. Conf. on Numerical Ship Hydrodynamics*, Berkeley, CA, 1976, University Extension, University of California, Berkeley, pp. 39–52.
29. G. R. Baker, D. I. Meiron and S. A. Orszag, 'Applications of a generalized vortex method to nonlinear free-surface flows', *Proc. 3rd Int. Conf. on Numerical Ship Hydrodynamics*, Paris, 1981, pp. 179–191.
30. T. F. Ogilvie, 'First- and second-order forces on a cylinder submerged under a free surface', *J. Fluid Mech.*, **16,** 451–472 (1963).
31. M. A. Grosenbaugh and R. W. Yeung, 'Flow structure near the bow of a two-dimensional body', *J. Ship Res.*, **33,** 269–283 (1989).